Synergistic effect of (3-Aminopropyl)Trimethoxysilane treated ZnO and corundum nanoparticles under UV-irradiation on UV-cutoff and IR-absorption spectra of acrylic polyurethane based nanocomposite coating

Synergistic Effect of (3-Aminopropyl)Trimethoxysilane Treated ZnO and Corundum Nanoparticles Under UV-Irradiation on UV-Cutoff And IR-Absorption Spectra of Acrylic Polyurethane Based Nanocomposite Coating

Mhd Abd Cader Mhd Haniffa[ab], Yern Chee Ching[a], Cheng Hock Chuah[b], Kuan Yong Ching[C], Liou Nai-Shang[d]

[a] Department of Chemical Engineering, Faculty of Engineering, University of Malaya, 50603 Kuala Lumpur, Malaysia

[b] Department of Chemistry, Faculty of Science, University of Malaya, 50603 Kuala Lumpur, Malaysia

[c]School of Foundation, University of Reading Malaysia, Persiaran Graduan, Kota Ilmu, Educity, 79200 Iskandar Puteri Johor, Malaysia

[d]Department of Mechanical Engineering, Southern Taiwan University of Science and Technology, 710 Tainan City, Taiwan, ROCa

HIGHLIGHTS

- Corundum and a secondary amine based APTMS coated ZnO nanoparticles were successfully synthesized.
- Charge-transfer activity and the intrinsic absorption property of corundum were observed under UV-irradiation exposure.
- The bonding between oxygen and an electrically inactive N atom along with their IR-absorption properties were observed after weathering study.
- UV and IR absorption of APTMS-ZnO based acrylic polyurethane nanocomposite coating (APUCs) are massively affected by the incorporation of corundum and M-SiO_2 nanoparticles respectively.

Abstract

ZnO and corundum (α–Al_2O_3) nanoparticles were successfully synthesized by aqueous precipitation and sintering techniques respectively. ZnO nanoparticles were effectively coated with

(3-aminopropyl)trimethoxysilane (APTMS) by polycondensation method to prevent the photocatalytic activity of ZnO during a UV-weathering study. X-ray diffractogram and FTIR were used to confirm the crystalline structure of as prepared nanoparticles, blue shift of the Al-O bond and the formation of a secondary amine via polycondensation of APTMS over ZnO surface. The prepared APTMS-ZnO, corundum and commercially available surface modified hydrophobic SiO_2 (M–SiO_2) nanoparticles were used to prepare the acrylic polyurethane (AP: Poly-Macrynal® SM 510N coating resign) bases nanocomposite coating on a polyurethane substrate. Individual and mixed nanoparticles were dispersed into acrylic polyurethane to prepare the coating layer on polyurethane film substrate separately. IR-active and UV-visible regions of the FTIR and UV-Vis spectroscopies were used to investigate the synergistic effect of the nanoparticles on a selected range of the radiative spectrum, especially the UV-resistant and IR-absorption properties of the coated films with and without exposure of UV-irradiations. Polyurethane substrate coated with APTMS-ZnO (2wt%) based acrylic polyurethane-based nanocomposite coating (APUC) layer containing 2 wt% corundum (D50) and 6 wt% M-SiO_2 (F50) exhibited 98.77% and 97.60% of UV-resistant property respectively. These results indicate that the visible light transparency and transmittance ability reduced significantly after 500h of UV-irradiation exposure. Both of the activity and deformation have great impact on the IR-absorption property of the APUC.

Keywords: UV-resistant; IR- absorption; Nanocomposite coating film; Corundum; APTMS-ZnO, charge-transfer activity.

1. Introduction

Radiative sky coolers are one of best invention that has been developed by several researchers and academics since 1972 in-order to preserve the energy consumption as they expected to reduce in near future. Radiative sky coolers absorb or reflect the ultra-violate (UV) and the infrared near- and mid-range portion of the solar spectrum due to the properties of their functional materials. Solar illumination brings 91.7% of the infrared radiation energy to the ground. This energy is concentrated in the wavelength range from 700~2500 nm while 8.3% is other electromagnetic radiation[1]. The objects convert 42.3% of the visible light and 49.4% of the near-infrared radiation energy of the solar radiation into heat, causing the temperature of the surface to increase[1]. Consequently, researchers and academics have developed materials to absorb and emit heat rays via different mechanisms.

Since 1972, there are number of materials have been used to satisfy the radiative cooling principle including; heat insulation materials such as hollow glass microspheres and / or hollow ceramic beads[2]; the IR-absorber or reflective material including SiO_2[3], titanium dioxide, tin oxide, antimony trioxide, magnesium oxide, zinc oxide, aluminum oxide and generally, antimony doped tin oxide (ATO), indium tin oxide (ITO), lanthanum hexaboride (LaB_6) and nanophotonic devices[4-10]; low heat absorbing transparent polymer resin called polymethyl-pentene (TPX)[2]. An inorganic metal oxide based effective multilayer nanophotonic device and a bilayer randomized glass-polymer hybrid metamaterial using TPX polymer matrix have been developed recently[2, 10]. A silver layer was deposited on one side of the hybrid metamaterial using an electron beam evaporator. To resist UV-radiation where they observed that the IR-absorption has depend upon the diameter of the microsphere[2]. On one hand, nanoscale materials have shown significant cooling ability while on the other hand microscale materials were used for the same. Both have cost effective and environmental issues. Consequently, it is utmost importance to study the ability to cutoff UV and IR- radiation using low cost and environmentally friendly materials. Nanomaterials and microscale materials provide a novel way to fabricate green composite materials for radiative cooling applications.

UV radiation is an utmost important factor which affect living organisms with having a wavelength shorter than 380 nm and commonly subdivided into UVA, UVB and UVC. Inorganic metal oxides such as TiO_2, ZnO, and CeO_2 are commonly used for this purpose rather than other organic UV absorbers due to their gradual embrittlement and undergoes rapid yellowing properties. However, photocatalytic activity of these metal oxides has degraded the polymer matrix of their nanocomposites coating films when they are exposed to UV-irradiations. Besides, UV-resistance materials itself have no ability to act as radiative cooling (below or above ambient temperature) materials. Consequently, IR-active material is required to make a complete radiative cooler.

Aluminum oxide (Al_2O_3) has been reported as radiative cooler below-ambient temperature [11]. Al_2O_3 is one of the metal oxides which can give different structural phases including γ-Al_2O_3, δ-Al_2O_3 and α-Al_2O_3. Al_2O_3 is a ceramic material showing great importance in many chemical and technological applications including optics, heat insulation, heat transfer, absorbent, antibacterial, biomedical *etc*. Thus beside other transition phases, corundum (α-phase of Al_2O_3) is the thermodynamically stable form of the Al_2O_3. The formation of the corundum can be described as a

hexagonal close packed sub-lattice of oxygen ions and an ordered array of Al^{3+} cations occupying 2/3 of the octahedral interstices[12]. Although, an intrinsic absorption of the corundum is expected to alternate the IR-absorption ability of the nanocomposite coating in the presence of UV-irradiation via charge transfer activity among their counter ions in the crystalline lattice. Furthermore, to the extent of our knowledge corundum has not yet been experienced with their IR-absorption activity as radiative cooler in the literature.

Numerous experimental methods have reported the preparation method of corundum. These include hydrolysis of aluminum alkoxides[13], chemical vapor deposition[14], thermal decomposition of aluminum alum[15], and thermal decomposition of inorganic aluminum salts[16, 17]. However, the heat treatment method such as calcination and sintering which are followed with dry or wet milling will give maximum purity of 99.6-99.9%[18, 19]. Further, when the temperature exceeds 1200 °C, the primary corundum particles will grow together to form three-dimensional aggregates. These pyrogenic corundum powders are generally ground by various grinders such as ball mill, jet mill and vibration mill to break their joints which form during sintering and to obtain monodispersed fine particles.

In this study (3-aminopropyl)trimethoxysilane (APTMS) has been used to coat the surface of the ZnO nanoparticles. The prepared corundum and commercially available surface modified SiO_2 (M-SiO_2) nanoparticles have been used to investigate the impact of mixed nanoparticles on UV and IR-absorptions properties of the nanocomposite coating compared with their individual performance. Commercial poly-macrynal-510n coating resin has been used as polymer matrix to investigate the stability of the nanoparticles after exposure to UV-irradiation. To assess the functional stability of the nanoparticles, the coated polyurethane (PU) films were exposed to UV-irradiations in a weatherometer for three consecutive cycles of UV-irradiations. The IR-active property of the corundum and M-SiO_2 nanoparticles become weaken, fade, and may lose their functions with respect to exposure of UV-irradiations. Consequently, different stoichiometric ratio of the respective APTMS-ZnO, corundum and M-SiO_2 nanoparticles have been embedded into the polymer matrix to coat PU film with different coating thickness. The synthesized nanoparticles are characterized by XRD, and FTIR. The effect of UV-irradiations on IR-active property of the corundum and M-SiO_2 embedded nanocomposite with and without APTMS-ZnO nanoparticle are

investigated via UV-visible and FTIR spectroscopy. Results have been compared before and after exposure of UV-irradiations using MRD-UV accelerated weathering chamber.

2. Material and methods

2.1. Materials

Synerburg Materail Co., Ltd provided polyurethane film (PU), Allnex Holding S.à r l. supplied poly-macrynal® sm 510n/60xmpac coating resin. Nippon Aerosil® Co., Ltd supplied surface modified (hydrophobic) crystalline free pyrogenic amorphous SiO_2 nanoparticles with a 12-14 nm particle size. (3-aminopropyl)trimethoxysilane, $Al(NO_3)_3.9H_2O$, $Zn(NO_3)_2.4H_2O$, Na_2CO_3, NaOH, 95% absolute ethanol were purchased from Sigma-Aldrich (Kuala Lumpur, Malaysia). All materials were used as received without any further purification.

2.2. . Synthesis of APTMS treated ZnO hybrid nanoparticles

The aqueous precipitation method was used to prepare ZnO nanoparticles as described previously [20] with some modification. In detail, zinc nitrate (0.5 M) was added drop by drop to the solution of 0.5 M sodium carbonate under vigorous stirring.

$$Zn(NO_3)_{2\,(aq)} + Na_2CO_{3\,(aq)} \xrightarrow[RT]{} ZnCO_{3\,(s)}\downarrow + 2Na^+_{(aq)} + 2NO_3^-{}_{(aq)} \quad (1)$$

$$ZnCO_{3\,(s)} \xrightarrow[650°C]{} ZnO_{(s)} + CO_{2\,(g)}\uparrow \quad (2)$$

The precipitate was then dried in an air circulating oven at 80 °C for 2 h, soon after separation from the solution using vacuum filtration by washing three times with distilled water and ethanol. The oven dried powder was calcined to 650 °C for 3h to obtain ZnO nano-powder. Finally, it was ball-milled at 200 rpm for 5h to get fine nano ZnO particles.

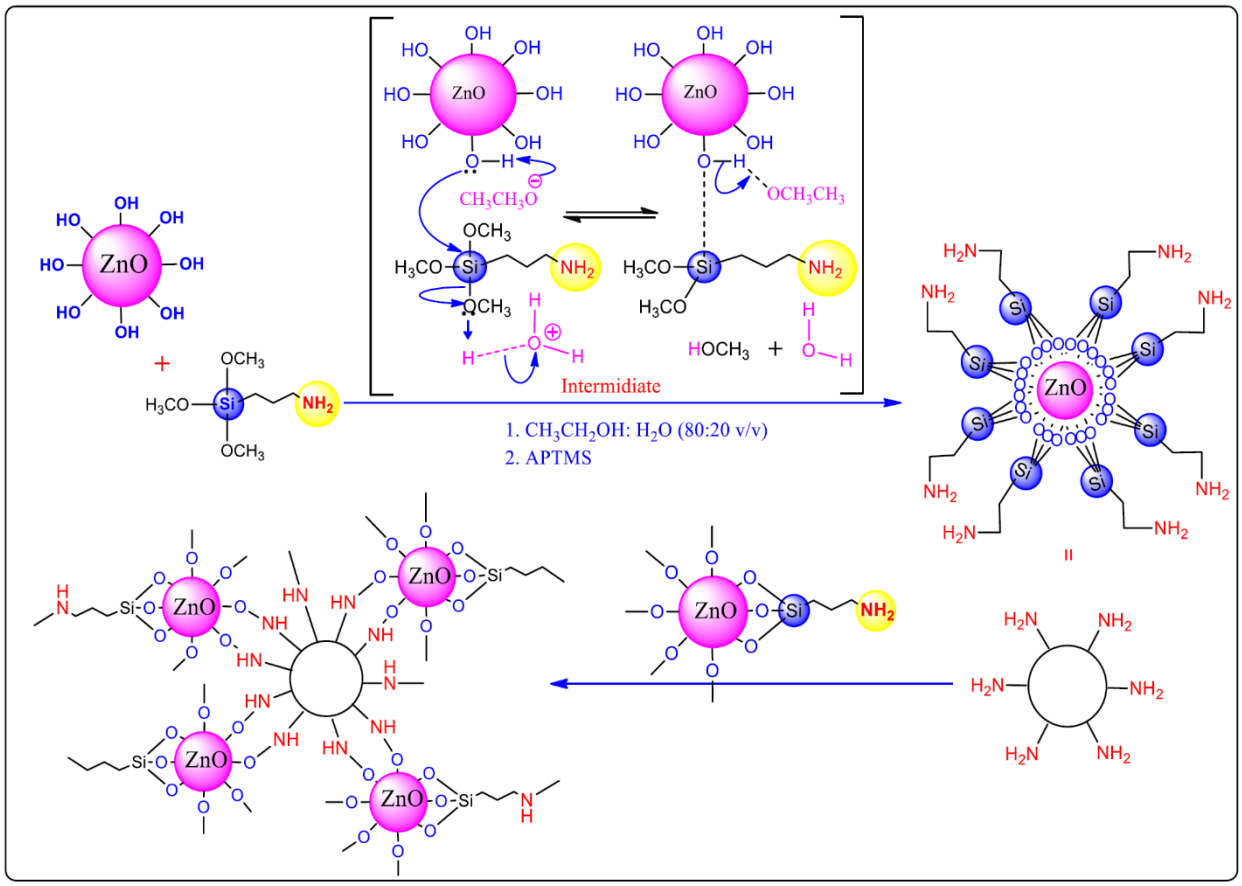

(3-aminopropyl)trimethoxysilane

Synthesis of APTMS treated ZnO hybrid nanoparticle was initiated with a dispersion of 3 g of as prepared ZnO nanoparticles into a 100 ml ethanol/distilled water mixture (80/20 (v/v)) for 30 minutes. Then, 2.05 g of APTMS was dropped into the ZnO dispersion and followed by 130 ml of 95% absolute ethanol and 70 ml of distilled water were added into the system. The reaction mixture was allowed to stir for 24 h at room temperature. Hybrid ZnO nanoparticles were filtered by gravity filtration and dried under room temperature for 12 h. Finally, dried hybrid ZnO nanoparticles were ball-milled at 200 rpm for 5 h. Scheme 1 illustrates the detailed reaction mechanism of the surface modification of the ZnO nanoparticles using graphical representation.

2.3. Synthesis of Corundum (α-Al_2O_3) nanoparticles

Step-sintering and ball-milling techniques were used to prepare the corundum nanoparticles via sol-gel method. Equations (4) and (5) describe the synthetic method of corundum nanoparticle formation. Aluminum nitrate ($Al(NO_3)_3 \cdot 9H_2O$, 25g) was transferred into a beaker containing 200

ml of distilled water. Sodium hydroxide solution (0.2 mol) was added drop by drop into the reaction mixture while maintaining the pH at around 6. The reaction mixture was stirred for 24 h at room temperature. Pure-white colored bayerite gel of $Al(OH)_3$ was obtained after washing with distilled water five times and filtered using gravity filtration. Filtrate was then dried in a freeze dryer and ball-milled for 24h at 200 rpm. The fine $Al(OH)_3$ nanoparticles were obtained after washing with distilled water five times and sintered by step-sintering up to 1350 °C with 10 °C/min heating rate at air. Finally, the obtained corundum particles were ball-milled at 200 rpm for 5 h.

$$Al(NO_3)_{3\,(aq)} + NaOH_{(aq)} \xrightarrow[pH=6]{} \underbrace{Al(OH)_3.xH_2O_{\downarrow}}_{\text{Bayerite gel}} \quad (4)$$

$$\underbrace{Al(OH)_3.xH_2O_{\downarrow}}_{\text{Bayerite gel}} \xrightarrow{\text{Freez dry}} Al(OH)_3\downarrow_{(s)} \xrightarrow[\substack{1.\ \text{Sintering}\\ 2.\ \text{Ball-milling}}]{} \alpha - Al_2O_{3\,(s)} \quad (5)$$

2.4. Preparation of nanocomposite coating formulation

Poly-macrynal resin (PMR, 50 g) consisting of 60% of solids was used to prepare the coating emulsion in a 50 ml solvent mixture of butanol and xylene (50:50 (v/v)). Respective nanoparticles embedded composite coating formulations were prepared using stoichiometric ratio given in Table 1. In order to achieve a better dispersion of the nanoparticles, all coating formulations were subjected to the non-ionic dispersing agent (Ethoxylated isodecyl alcohol (EIA)), ultrasonication and mechanical stirring.

1. APTMS-ZnO nanoparticles (2 wt%), EIA (0.5 ml) and diluted PMR were stirred for 1 h at 1150 rpm followed by ultrasonication for 20 min to obtain a better coating formulations.

2. Corundum nanoparticles (2 wt%), EIA (0.5 ml) and diluted PMR were used to fabricate the IR-active coating with same process which had been used to disperse the nanoparticles as above.

3. M-SiO_2 nanoparticles (2 wt% and 6 wt%) were used to prepare the IR-absorbing coating incorporated with EIA (0.5 ml) and diluted PMR. The dispersion process was same as before.

2.5. Coating process

The coating was conducted using Meyer rod method as described previously[21]. Transparent PU film was used as support for the process, where the nanoparticles embedded coating formulations were applied on the PU surface. Nos. 10, 25 and 50 rods were used to make the coatings on the PU film to get 10 µm, 25 µm, and 50 µm coating thickness. We also did apply coatings with two different combinations of APTMS-ZnO: corundum, and APTMS-ZnO: M-SiO_2 composite. The study is to investigate the UV-resistant of the coating and the impact of APTMS-ZnO nanoparticles on functional stability of the corundum and M-SiO_2 nanoparticles after exposure of UV-irradiations. The coated PU films were then leave to dry under room temperature.

Table 1
The stoichiometric ratio of the nanoparticles and AP based nanocomposite coating formulations.

Sample code / Coating thickness			Stoichiometric ratio of the Nanoparticles (w/w %)			Coating formulation/ wt%
10 µm	25 µm	50 µm	APTMS-ZnO	Corundum	M-SiO_2	
A10	A25	A50	2	-	-	98
B10	B25	B50	-	2	-	98
C10	C25	C50	-	-	2	98
D10	D25	D50	2	2	-	96
E10	E25	E50	2	-	2	96
F10	F25	F50	2	-	6	92
Control			-	-	-	100

The average coating thickness was calculated as described previously using the equation given below. The weight of the coating was calculated from the difference between the weight of the PU film before and after coating. Rule of mixture method was used to calculate the density of the coating.

$$\text{Average coating thickness} = \frac{\text{Weight of the coating}}{\text{Density of the coating}} \quad (6)$$

2.6. Weatherometer

MERIDIAN UV weathering chamber (MRD-UV-SF, MERIDIAN, Malaysia) was used to investigate the outdoor exposure and the coating stability of the coated PU films. Accelerated

weathering tests were performed based on ASTM G154 standard practice, where florescent lamps with 313 nm wavelength of UV-irradiation were used to achieve 8 hours weathering cycles. APUC samples were exposure under UV-irradiations for 4 h at 70 °C followed by 4 h of condensation at 50 °C.

2.7. Material characterization

2.7.1. X-ray diffractogram analysis

X-ray diffraction (XRD) pattern of the nanoparticles were analyzed using Siemens D5000 system. Monochromatic Ni-filter was used to X-ray the samples using Cu Kα radiation with a wavelength of 1.542 Å. The diffracted intensity data were measured between the ranges of $20° \leq 2\theta \geq 80°$, using 0.05° scan steps with a counting rate of 1.5°/min while, the generator was operated at 40 kV and 40 mA.

2.7.2. Fourier transfer infrared (FTIR) spectroscopic analysis

FTIR spectroscopy was conducted using PerkinElmer Spectrum 400 FTIR spectrometer unit (PerkinElmer, Waltham, MA, USA) with the resolution of 4 cm^{-1} and 32 scans per recording. KBr pellet technique was used to characterize the nanoparticles and the KBr pellets were replaced by sample specimen of the films in the sample holder with same dimeter to study the IR-absorption property.

2.7.3. UV-resistance analysis

The UV absorption and transmission properties of all APTMS-ZnO nanoparticles embedded APUCs were measured by using U-2810 UV-vis spectrophotometer (Hitachi, Japan). The measurements were taken in the range from 200nm to 400 nm and 400 nm to 1400 nm respectively and compared with neat coating film (without embedding of nanoparticles).

2.7.4. *Investigation of UV and IR-absorption properties of the APUC*

FTIR and UV-visible spectroscopy were used to investigate the functional stability of the nanoparticles before and after exposure of UV-irradiations. All coated PU films were exposed to UV-irradiation for 24 h, 168 h and 500 h by three sets of fifteen samples. The first set of fifteen samples was UV-irradiated for 24h, the second was 168h and finally set was 500 h. Neat coating

was also performed on PU films and exposed them to accelerated weathering test in MERIDIAN UV weathering chamber with APUCs.

3. Results and discussion

FTIR spectroscopy and XRD methods were used to confirm the surface modification of ZnO nanoparticles and phase transformation of the corundum nanoparticles. The formation of corundum and the APTMS-treatment of ZnO nanoparticles have investigated by FTIR. Crystalline nature of the prepared nanoparticles was confirmed by XRD. In order to understand the UV and IR-absorption properties of the APUC, the nanoparticles embedded coated PU films were investigated using FTIR and UV spectroscopies via selected regions. The investigation was performed with respect to different coating thickness before and after exposure of UV irradiations. Moreover, impact of corundum and M-SiO_2 nanoparticles on transmittance, visible-shielding ratio (VR), and UV-blocking ratio (UVR) of the APUC were observed by UV-visible spectroscopy. The observation was done in the selected wavelength before and after consecutive exposure of UV-irradiations and compared with blank PU film.

3.1. FTIR analysis for the confirmation of nanoparticles preparation

FTIR spectra of ZnO nanoparticle and their APTMS functionalization were illustrated in Fig. 1A. According with the previous reports, it is believed that the respective absorption bands at 3459 and 500 cm^{-1} of ZnO nanoparticle's spectrum are attributed to the hydroxyl (-OH) and Zn-O stretching vibrations[22, 23]. On the other hand, upon APTMS interaction, the -OH band is broadened and shifted to 3410 cm^{-1} with single broad band is observed at 3249 cm^{-1} originating from the stretching vibrations of the –N–H group of secondary amine as illustrated in the scheme 1. Note that, the FTIR spectrum of APTMS-ZnO was not exhibited two consecutive bands below 3300 cm^{-1}. These bands are attributed to stretching vibration of the N–H group of primary amine. Another two newly formed consecutive bands was observed at 2932 and 2884 cm^{-1}, originated from symmetric and asymmetric C–H stretching vibrations of alkyd chain of the APTMS. After APTMS functionalization the presence of secondary amine group on the surface of ZnO nanoparticles was investigated on their FTIR spectrum. The band at 1582 cm^{-1} attributed to the bending vibration of N–H group has been confirmed in the investigation.

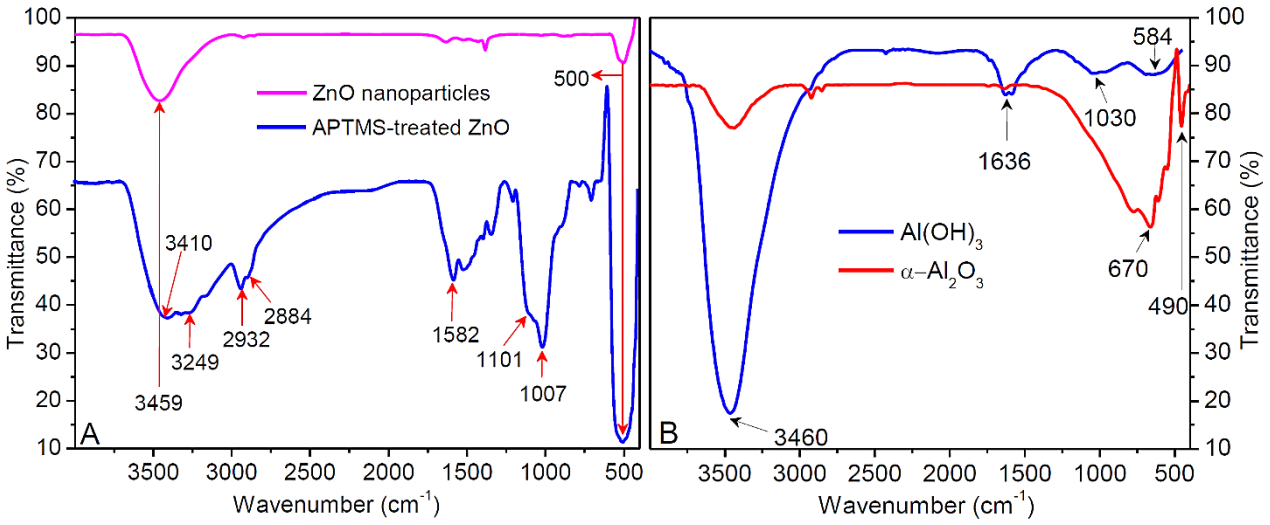

Fig. 1. FTIR spectra of; (**A**) As prepared ZnO and their APTMS treated ZnO nanoparticles; (**B**) freeze dried $Al(OH)_3$ and their phase transformation (corundum) after sintering and ball milling treatments.

In addition, the strong broad and sharp consecutive bands at 1101 and 1007 cm^{-1} are attributed to symmetrical stretching vibrations of the Zn–O–Si and Si–O–Si bonds. Observation of these bonds has also been confirmed that the amino-silane of APTMS is covalently bound with the –OH groups of the ZnO surface as exhibited in sheme1.

The formation of corundum was confirmed by FTIR spectroscopy. Fig. 1B exhibits the spectra of the $Al(OH)_3$ and their phase transformation into corundum. A broad sharp peak was observed at 3460 cm^{-1}, which is attributed to stretching vibration of –OH groups in the $Al(OH)_3$. It is observed that the FTIR absorption band at around 1636 cm^{-1} was attributed to the freeze dried $Al(OH)_3$. Also, it is a well-known band of H–O–H angle bending vibration of weakly bounded molecular water. The corresponding peak was observed at the same place in previous work where it was remained in their samples at different temperatures up to 1000 °C [24]. However, it was not observed in this FTIR spectrum of corundum as shown in Fig. 1(a). This might be caused by high sintering temperature at 1350 °C. The following sequence of the successive thermal treatments has describing the phase transformations of Al_2O_3.

$$Al(OH)_3 \xrightarrow[400^{\circ}C]{} a-Al_2O_3 \xrightarrow[\text{2. Red Shift}]{\text{1. 500 °C}} \gamma-Al_2O_3 \xrightarrow[\text{2. Red Shift}]{\text{1. 800 °C}} \delta-Al_2O_3 \xrightarrow[\text{2. Blue Shift}]{\text{1. 1000 °C}} \theta-Al_2O_3$$

$$\xrightarrow[\text{2. Blue Shift}]{\text{1. 1200 °C}} \alpha-Al_2O_3$$

The other two absorption bands such as 1030 and 584 cm^{-1} were attributed respectively to the (OH)–Al–(OH) asymmetric stretching vibration and Al-O stretching mode of the octahedral coordination of the $Al(OH)_3$. Moreover, Al-O stretching mode of the tetrahedral coordination was not observed within the region of 750-850 cm^{-1}. On the other hand, it is believed that the FTIR spectrum of corundum exhibits a strong arguments of the $Al(OH)_3$ phase transformation into corundum via strong sharp bands at 670 and 490 cm^{-1}. The respective bands were attributed to the stretching mode of Al-O in an octahedral coordination where it was reported in the range of 500-750 cm^{-1} and the blue shift due to size confinement effect from 584 cm^{-1} ($Al(OH)_3$) to 490 cm^{-1} (corundum). The hexagonal closest packed lattice structure of the corundum has been confirmed via absents of (OH)-Al-(OH) asymmetric stretching vibration at 1030 cm^{-1} and the red shifts where they are reported from 550 (γ-Al_2O_3) cm^{-1} to 520 (δ-Al_2O_3) cm^{-1} which can form at below 1000 °C. Consequently, the formation of red shift due to dangling bonds on the surface of corundum has been limited at high temperature of 1350 °C.

3.2. XRD analysis of the surface treated nanoparticles

Structural characterizations of APTMS-ZnO and thermally cultured corundum nanoparticles have been performed using XRD as illustrated in Fig. 2. The XRD pattern of the APTMS-ZnO is shown in Fig. 2A and the spectrum exhibits the typical peaks at 2θ = 31.7°, 33.9°, 36.2°, 47.3°, 56.4°,62.7°, 67.3°, 68.2°, 69.4° and 72.4° attributed to the planes (1 0 0), (0 0 2), (1 0 1), (1 0 2), (1 1 0), (1 0 3), (2 0 0), (1 1 2), (2 0 1) and (0 0 4) respectively, which can be index to quartzite hexagonal ZnO structure. Furthermore, it also demonstrates good agreement with ZnO standard hexagonal crystal system of ref pattern JCPDS 01-079-0205 and with the lattice constant of a = 3.2417, b = 3.2417 and c =5.1876 Å. The results exhibit good agreement with the results reported from previous works [25]. In deeply, there are no more peaks and corresponding planes were observed after surface treatment with APTMS/ZnO composite coating.

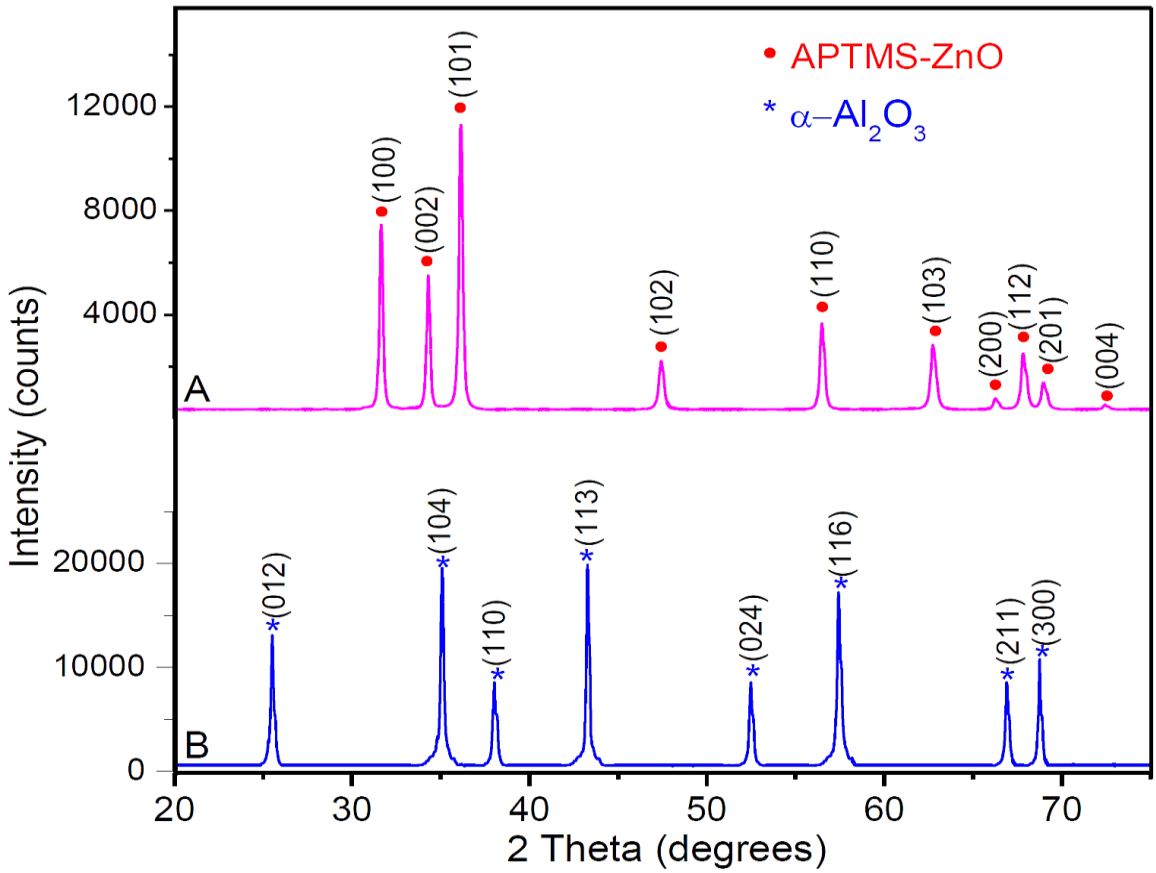

Fig. 2. XRD spectra of (**A**) APTMS treated (basic condition) ZnO nanoparticles; (**B**) phase transformed corundum after sintering at 1350 °C with 10 min of holding temperature and ball milling at 200 rpm for 5h.

However, APTMS-ZnO exhibits an improved peak intensities compared with ZnO nanoparticles. These results can only be explained by the surface functionalization of ZnO via APTMS. It is also observed that the corresponding peaks of the APTMS-ZnO have been broadened after APTMS based functionalization. The same observations have been reported elsewhere previously [25-27]. Consequently, these results confirmed that the surface of ZnO nanoparticles will not influence the crystalline phases of the affixed molecules.

The XRD patterns obtaining from corundum are displayed in Fig. 2B. The figures illustrate that the characteristic peaks of corundum at around 2θ = 25.45°, 35.07°, 37.96°, 43.23°, 52.48°, 57. 40°, 66.95° and 68.74° are corresponding to the respective planes of (0 1 2), (1 0 4), (1 1 0), (1 1 3), (0 2 4), (1 1 6), (2 1 1) and (3 0 0).These have perfectly agreed with corundum standard hexagonal

crystal system of ref pattern JCPDS 98-003-0024 and the lattice constant of a = 4.7760, b = 4.7760 and 13.0100 (Å).

3.3. Spectroscopic analysis before UV-weathering study

Nanoparticles embedded APUCs were characterized by FTIR and UV-visible spectroscopy before exposure of UV-irradiations. Spectroscopic analysis has been conducted based on the IR-absorption ability of the APUCs with respect to coating thickness. Moreover, individual nanoparticle based APUCs and mixed nanoparticles APUCs have also been analyzed. Best IR-absorbing coating composition has been used to study the impact of corundum and M-SiO_2 nanoparticles on UV-resistant property of the APTMS-ZnO embedded APUCs.

3.3.1. FTIR spectral analysis of the individual nanoparticles embedded APUCs

Fig. 3 shows the IR-absorption ability of the nanocomposite embedded PU films with respect to different coating thickness within selected region. Corresponding peaks in the range of 3600 to 3250 cm^{-1} on the right side of the Fig. 3(a), (b) and (c) are attributed to (a) the broadening of all antisymmetric stretching vibration of –OH and N-H groups which are contributed by secondary amine of the APTMS-ZnO and the polymer matrix [22, 28]; (b) and (c) all antisymmetric vibration of –OH and N-H groups contributed by polymer matrix [22] form via molecular interaction between the nanoparticles and the coating matrix. On the other hand, peak intensity of the selected IR region from 1400 to 800 cm^{-1} of the spectra has been increased with the accumulations of nanoparticles.

There are four consecutive peaks have been observed within the selected region at around 1377, 1232, 1182 and 1089 cm^{-1} which are attribute to symmetric bending of aliphatic CH_3 (–C–H), stretching vibrations of –C–N and –N–H groups in amide, the –C–H bending mode with –C–C inter-chain stretching mode, and stretching vibrations of –C–O in –O–CH_2 [29-32] respectively. It is believed that the accumulation of corundum into nanocomposite has reflected IR-spectrum. Fig. 3(b1) has clearly shows that the absorption peak area decreases when the coating thickness of the corundum embedded APUCs increases from 25µm to 50µm. Especially, APUCs with 25 µm exhibits more absorption peak area compared to 50 µm coatings. On the other hand, absorption peak area of Fig. 3(c1) has been enlarged compared to Fig. 3(a1) and (b1). This is because of the IR-absorption ability of the oxygen atom presents in –Si–O bonds of the APUCs. The

corresponding IR-absorption peaks of the oxygen atom was found at around 1089-1106 cm^{-1} as illustrated via circle in Fig. 3(c1) [3].

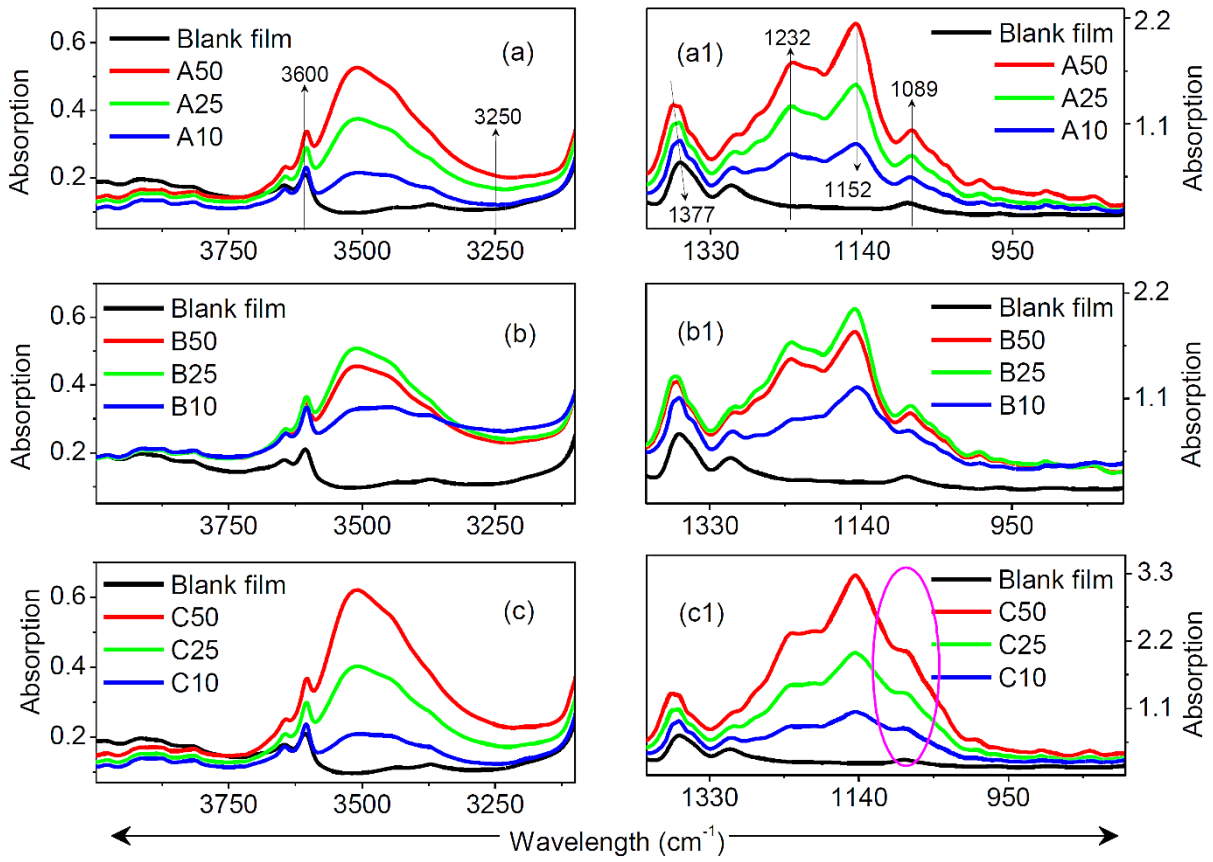

Fig. 3. FTIR spectra of a selected range from 4000 to 3000 cm^{-1} and 1520 to 760 cm^{-1} of the nanocomposite coated films with different coating thickness (10, 25 and 50 µm) with respect to individual nanoparticles. Nanocomposite coating embedded with (a) & (a1): 2 wt% of APTMS-ZnO; (b) & (b1): 2 wt% of corundum and (c) & (c1): 2 wt% of M-SiO_2.

3.3.2 FTIR spectral analysis of the mixed nanoparticles embedded APUC

Thermal mutation of the mixed nanoparticles embedded APUCs have been investigated via FTIR spectroscopy within the selected region with respect to coating thickness as illustrated in Fig. 4. IR-absorption ability of the APTMS-ZnO and corundum embedded APUCs (Fig. 4(d1)) have been reduced by half compared to the mixing of M-SiO_2 in both 2 wt% and 6 wt% with APTMS-ZnO as illustrated in Fig. 4(e1) and (f1). It might be due to thermal insulation property of the corundum [33].

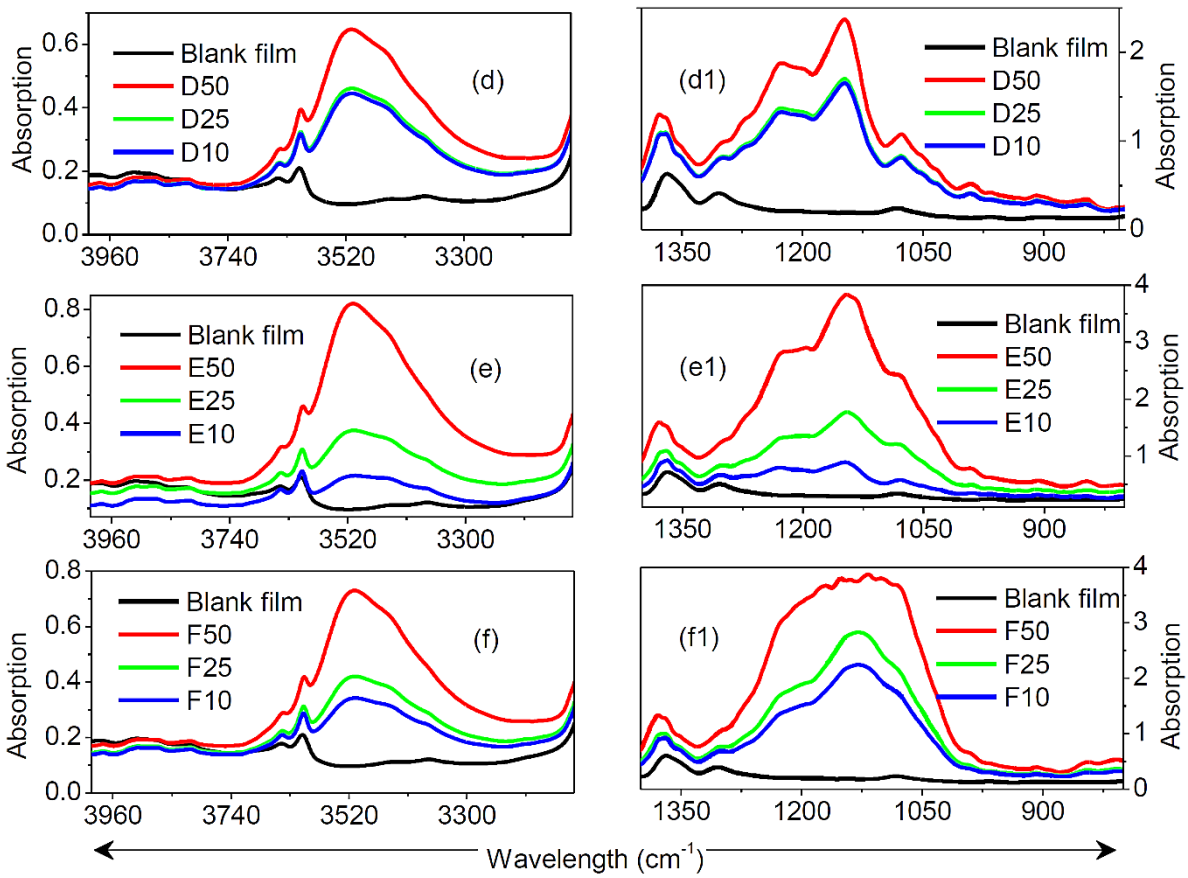

Fig. 4. FTIR spectra of a selected range from 4000 to 3000 cm^{-1} and 1520 to 760 cm^{-1} of the APUCs with different coating thickness (10, 25 and 50 µm) with respect to different embedded mixed nanoparticles, (d) and (d1): APTMS-ZnO and corundum 2:2 (w/w); (e) and (e1) E: APTMS-ZnO and M-SiO_2 2:2 (w/w) and (f) and (f1): APTMS-ZnO and M-SiO_2 2:6 (w/w).

3.3.3 FTIR spectral analysis of the individual and mixed nanoparticles embedded nanocomposite coating films

Impact of mixing the thermal mutating nanoparticles on IR-absorption of the APUCs has been investigated through FTIR spectra as exhibited in Fig. 5. Compared with A50: APTMS-ZnO and B50: corundum nanoparticles embedded APUCs, the films with mixed nanoparticles D50: APTMS-ZnO and corundum 2:2 (w/w) embedded APUCs exhibit significant enhancements in IR absorption for both selected region of the FTIR spectra as illustrated in Fig. 5(g) and (g1). However, APTMS-ZnO and M-SiO_2 based APUC exhibit greater IR-absorption peak intensity than APTMS-ZnO and corundum nanoparticles based APUC as illustrated in Fig. 5(h) and (h1).

Moreover, even better improvement in IR-absorption of the APUC was illustrated in Fig. 5(i) and (i1) where 6 wt% of M-SiO_2 was mixed with 2 wt% of APTMS-ZnO for the coating process.

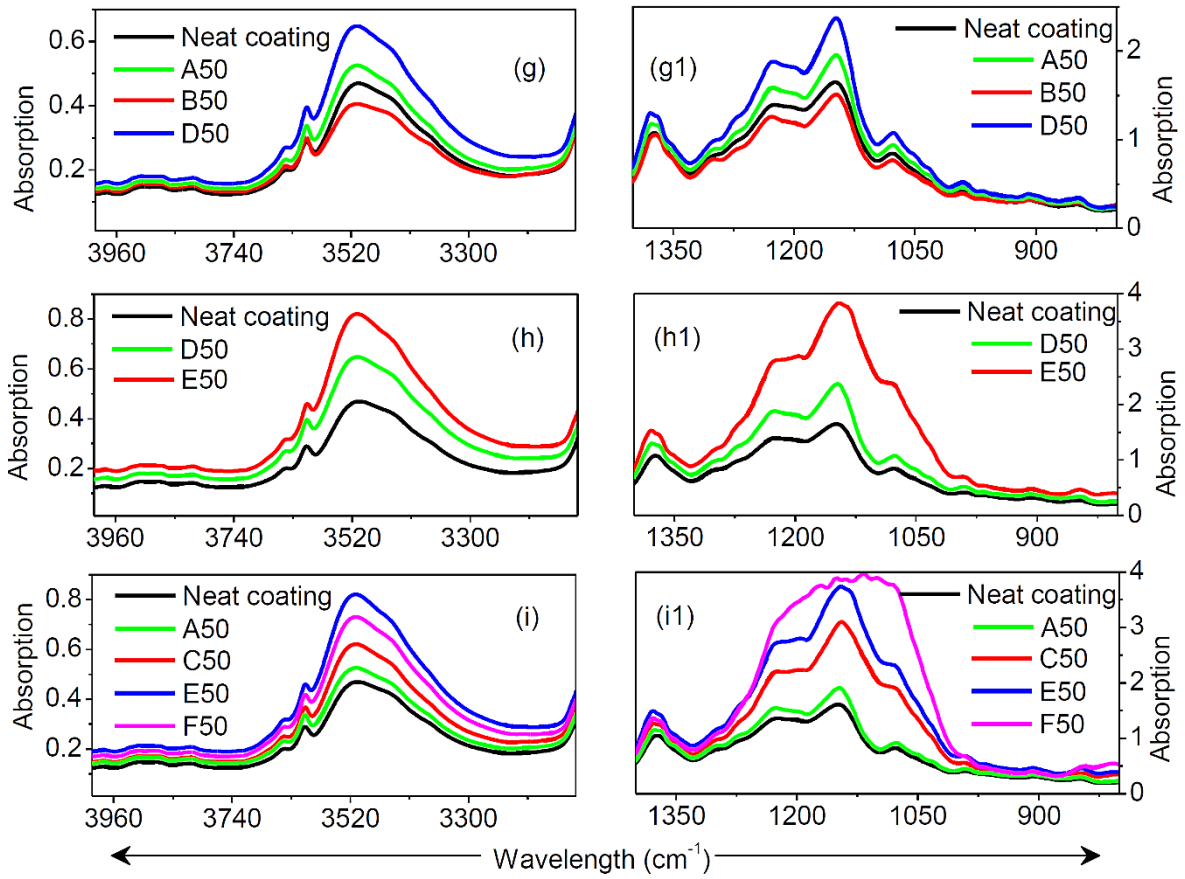

Fig. 5. FTIR spectra of a selected range from 4000 to 3000 cm^{-1} and 1520 to 760 cm^{-1} of the nanocomposite coated films with 50 µm coating thickness. Comparison analysis between nanocomposite with individual and mixed nanoparticles (g) and (g1): A50 (APTMS-ZnO), B50(corundum) and D50 (APTMS-ZnO and M-SiO_2 2:2 (w/w)); (h) and (h1) E50 (APTMS-ZnO and M-SiO_2 2:2 (w/w)) and (i) and (i1) C50 (2 wt% of M-SiO_2) and F50 (APTMS-ZnO and M-SiO_2 2:6 (w/w))

.

3.3.4 UV-visible spectroscopic analysis for individual and mixed nanoparticles embedded nanocomposite coating

Individual and mixed nanoparticles embedded composite coating films were tested with UV-visible spectroscopy to understand the UV-resistant property of the APUCs. Fig. 6 illustrates the

impact of mixed nanoparticles on UV-resistant property compared with individual nanoparticles embedded APUCs. UV-absorption peak was observed at 374 nm in all tested samples as illustrated in Fig. 6.

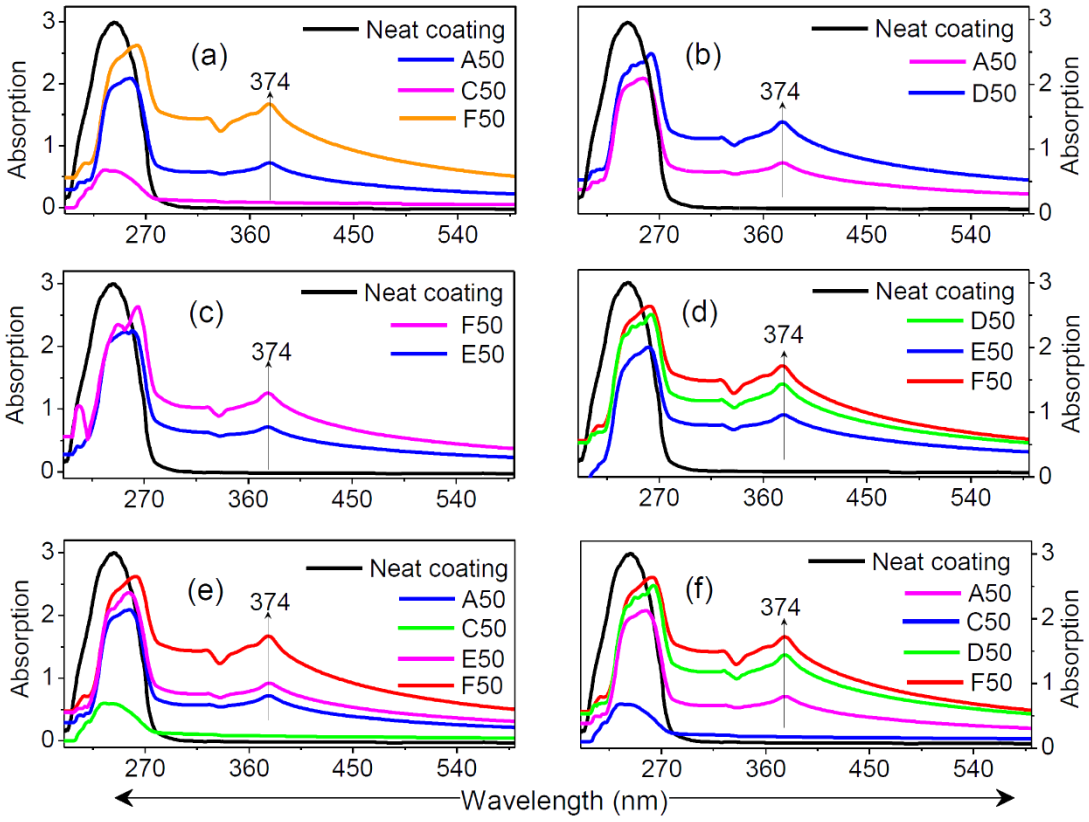

Fig. 6. UV-visible spectra for selected range from 600 to 200 nm of the nanocomposite coated films with 50 µm coating thickness and comparison analysis between nanocomposite coating embedded with individual and mixed nanoparticles A50: 2 wt% of APTMS-ZnO; C50: 2 wt% of M-SiO_2; F50: APTMS-ZnO and M-SiO_2 2:6 (w/w); D50: APTMS-ZnO and corundum 2:2 (w/w); E50: APTMS-ZnO and M-SiO_2 2:2 (w/w).

It is believed that the C50: M-SiO_2 embedded nanocomposite coating has exhibited very weak UV-resistant property as shown in Fig. 6(a), (e) and (f). In contrast, absorption property was improved after mixed with 2wt% of APTMS-ZnO as illustrated in Fig. 6(a). The sample F50: APTMS-ZnO and M-SiO_2 2:6 (w/w) exhibits better UV-resistant property compared to the sample A50 incorporated with only 2wt% of APTMS-ZnO nanoparticles. We observed the same phenomenon in the sample D50 containing with APTMS-ZnO and corundum 2:2 (w/w) which can also be compared with sample A50 as illustrated in Fig. 6(b). Furthermore, Fig. 6(c) exhibits

improvements in UV-absorption property was observed in APUCs embedded with different weight percentages of M-SiO_2 nanoparticles. The samples with same weight percentage of M-SiO_2 and corundum exhibited different UV-apportion property as shown in Fig. 6(d). Sample D50 with 2:2 (w/w) of APTMS-ZnO and corundum nanoparticles exhibited better UV-apportion property compared to the sample E50 with 2:2 (w/w) of APTMS-ZnO and M-SiO_2. Moreover, the same trend of improvements was observed in Fig. 6(e) and (f).

3.4 Spectroscopic analysis after UV-weathering study

UV-weathering study has been performed to understand the IR and UV absorption ability of the APUCs and their future applicability as the functional components for radiative cooler. Three consecutive cycles including 24 h, 168 h and 500 h have been used to scrutinize the IR and UV absorption ability. According to previous spectroscopic analysis results, the mixed nanoparticles embedded APUCs with 50 µm coating thickness have only been used for this weathering study. IR and UV-absorption properties as well as their transmittance ability of the tested APUCs were investigated as soon as possible after completion of each UV-irradiation cycles.

3.4.1 FTIR spectral analysis of the nanocomposite coatings after UV-weathering study

Fig. 7 shows the migration pattern of IR-absorption of the nanoparticles embedded APUCs with respect to continuous UV-weathering cycles. The improvement in IR-absorption ability was observed after 500 h cycle compared to other cycles (24 h, and 168 h) of UV-irradiations. The impartments were observed in the sample D50 containing 2:2 (w/w) of APTMS-ZnO and corundum as well as in sample E50 containing 2:2 (w/w) of APTMS-ZnO and M-SiO_2 as illustrated in Fig. 7(a1) and (b1). However, it is believed that the accumulation of M-SiO_2 might contribute to the same IR-absorption pattern in all the time of UV-exposure as shown in Fig. 7(c1). In contrast, Fig. 7 (a1) and (b1) shows weak IR-absorption in samples D50 and E50 after 168h than 24h of UV-irradiation. In one hand, it may be due to charge-transfer activity of the nitrogen atoms in APTMS-ZnO with corundum nanoparticle. Consequently, the sample D50 shows significant reduction in IR-absorption as illustrated in Fig. 7(a1) after 168 h of UV-irradiations. However, the IR-absorption has increased after 500 h of UV-irradiation due to the intrinsic absorption edge of

the corundum nanoparticles [34]. On the other hand, sample E50 shows significant reduction of IR-absorption due to the deformation of M-SiO_2 nanoparticles into nonlinear Si_2O which could bonded with an electrically inactive N from APTMS-ZnO [35] and enhance the peak intensity in both selected regions as illustrated in Fig. 7(b) and (b1).

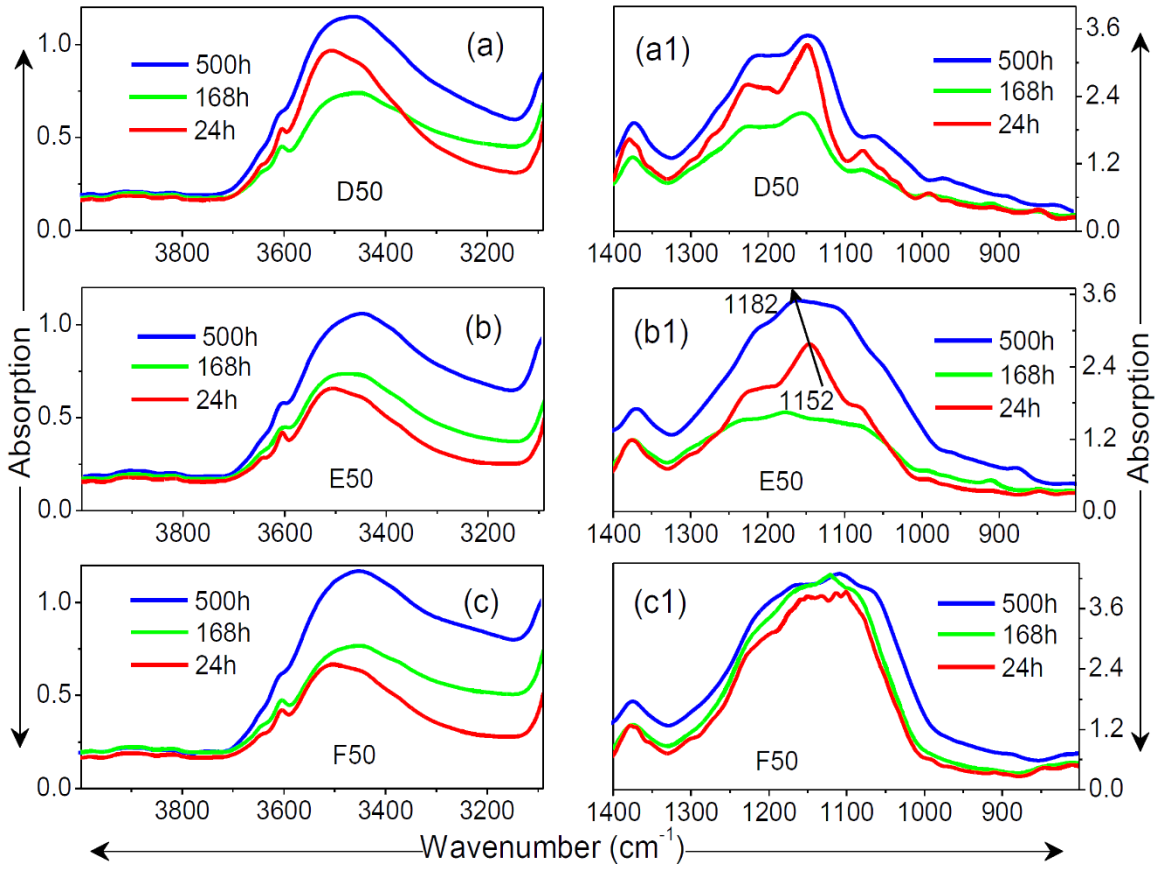

Fig. 7. FTIR spectra for selected range from 4000 to 3000 cm^{-1} and 1520 to 760 cm^{-1} of the nanocomposite coatings with 50 µm coating thickness. Comparison analysis between UV-weathering cycles of nanocomposite caoating embedded with (a) & (a1): D50 (APTMS-ZnO and corundum 2:2 (w/w)); (b) & (b1): E50 (APTMS-ZnO and M-SiO_2 2:2 (w/w)) and (c) & (c1): F50 (APTMS-ZnO and M-SiO_2 2:6 (w/w)).

The experimental evidence has proved that "If the oxygen were bonded to some other electrically inactive atom X, the O–X stretching vibration would also be infrared active"[36, 37]. In fact, IR-absorption of the sample E50 has been increased after 500 h of UV-irradiation exposure. This significant enhancement has also been confirmed by the peak shifting from 1152 to 1182 as illustrated in Fig. 7(b1) which was attributed to Si=O stretching frequency [3, 38, 39].

Antisymmetric stretching vibration of –OH and N-H groups are contributed by the secondary amine from the APTMS-ZnO and the polymer matrix [22, 28] which have been increased as shown in Fig. 7(a), (b) and (c) after 500 h of UV-irradiation exposure.

3.4.2 UV-visible spectroscopic analysis of the nanocomposite coatings after UV-weathering study

After exposure of UV-irradiation, the samples were used to study the UV-resistance ability within the range from 200 to 1400 nm. UV-absorption property of the tested samples have shown different phenomena as illustrated in Figure 8.

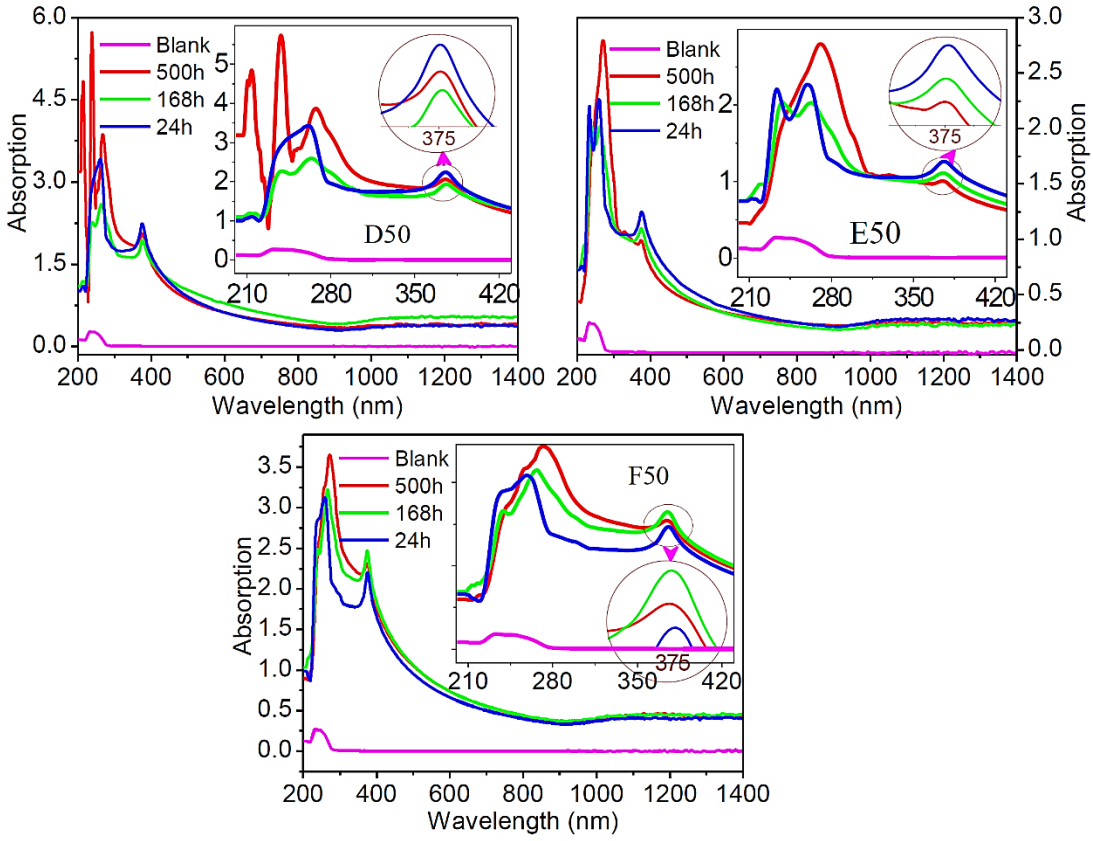

Fig. 8. UV-visible spectra of the nanocomposite coatings with 50 µm coating thickness after weathering study. Comparison analysis among weathering cycles of nanocomposite coating with mixed nanoparticles D50: APTMS-ZnO and corundum 2:2 (w/w); E50: APTMS-ZnO and M-SiO_2 2:2 (w/w) and F50: APTMS-ZnO and M-SiO_2 2:6 (w/w).

Figure 8 shows that the sample D50 reduction in the UV-absorption ability at the beginning but enhanced after 500 h of UV-irradiation as illustrated in Fig. 8. This might be due to the charge transfer activity of the nitrogen atoms in APTMS-ZnO with corundum nanoparticle and intrinsic absorption edge of the corundum nanoparticle [34]. On the other hand, Fig. 8 exhibits lower UV-absorption ability in sample E50 which embedded with 2 wt% of M-SiO_2. However, the sample F50 with 6 wt% of M-SiO_2 has shown improved UV-absorption ability after 500 h of UV-irradiation.

3.4.3 Transmittance analysis of the nanocomposite coatings after UV-weathering study

The transmittance pattern of the APUCs after three consecutive exposures of UV-irradiations was investigated by using transmittance, visible-shielding ratio (VR), and UV-blocking ratio (UVR) properties of the tested samples. The VR and UVR of the APUCs have been analyzed using the Equation 7 below [40,41].

$$R(\%) = \left(1 - \frac{T}{T_0}\right) \tag{7}$$

where T_0 is the transmittance of blank and T is the transmittance of the APUCs.

Impact of corundum and M-SiO_2 on UV-resistance and transmittance was investigated through UVR, VR and transmittance as described in previous studies [38]. The results of the UV-blocking ratio, visible-shielding ratio and transmittance of the nanocomposite coating sample of D50, E50 and F50 were listed in Table 2. High visible light transparency and excellent UV-resistance properties of these nanocomposites film have made them desirable for a wide range of outdoor applications [42, 43, 44, 45]

Table 2
The UV-blocking ratio, visible-shielding ratio and transmittance of the nanocomposite coating films

Samples	UV-I/ h	T(%) 550	VR(%) 550	UVR(%) 300	UVR(%) 225
D50	RT	76.83	38.14	89.71	61.78
	24	60.47	53.48	95.78	77.28
	168	47.29	58.60	95.98	80.37

	500	56.81	52.46	98.77	80.48
E50	RT	87.52	19.31	76.88	83.39
	24	73.12	36.51	88.59	95.19
	168	77.36	28.42	89.60	92.47
	500	70.72	27.40	95.11	97.48
F50	RT	70.31	38.78	91.87	81.06
	24	57.63	54.27	95.02	89.63
	168	51.87	57.37	97.19	89.46
	500	52.16	57.72	97.60	81.60

UV-I = UV-irradiation, T = Transmittance, VR = visible-shielding ratio, UVR = UV blocking ratio, RT = room temperature.

The room temperature UVR of APUC was increased with an incorporation of corundum (sample D50) compared to the same amount of M-SiO_2 (sample E50). APUC exhibited 91.87% of UVR with the introduction of 6wt% of M-SiO_2 (sample F50) at 300 nm. However, the UVR of the samples D50 and E50 were increased up to 98.77% and 95.11% respectively at 300 nm. In contrast, sample E50 exhibited higher UVR up to 83.39 % at 225 nm compared to samples D50 and F50. In general, the tested samples had shown increasing trend of UVR for both of the 300 and 225 nm with respect to different UV-irradiation cycles [46]. It is believed that the respective charge transfer activity of the nitrogen atoms in APTMS-ZnO with corundum nanoparticle and the deformation of M-SiO_2 into nonlinear Si_2O have impacted significantly on the VR of the samples D50 and E50 respectively. Nevertheless, VR property of the sample F50 was enhanced up to 57.72% after 500 h of UV-irradiations exposure. Besides, sample E50 also exhibits higher visible light transparency and UV-resistant efficiency than sample F50. The high UV and visible light absorption has caused less transparency on sample D50.

4. Conclusion

The nanosized of ZnO and corundum particles were successfully synthesized using sophisticated two steps routines with high yield. The obtained ZnO powders were coated with APTMS and its effect on the UV and IR spectrum of the APUC coating containing corundum and M-SiO_2

nanoparticle were studied. The following conclusions can be drawn from the investigation and spectral analysis in this study.

1) Surface coating of ZnO nanoparticles via APTMS is depend upon the reaction time where the coating can produce primary and secondary amine on ZnO nanoparticle surface. The surface coated ZnO can be used as reinforcement or crosslink for a wide range of industrial applications.

2) Synthesis of corundum nanoparticles is desirable at pH=6 under aqueous precipitation routine, freeze dryer, sintering and ball-milling techniques. The prepared corundum nanoparticles have shown a strong Al–O blue shift at FTIR spectra.

3) APUC has exhibited an improved IR and UV-absorption ability with the incorporation of corundum and M-SiO_2 nanoparticles, M-SiO_2 nanoparticles also enhance the IR and UV absorptions of APUC coating with respect to weight percentage of M-SiO_2. However, the transmittance of IR and UV reduces after UV-irradiations weathering.

4) Charge transfer activity of the nitrogen atoms in APTMS-ZnO with corundum nanoparticle and the deformation of M-SiO_2 into nonlinear Si_2O might occur when the samples expose to UV-irradiations. Consequently, our experimental is an initiative pathway to investigate the involvement of the corundum nanoparticle into charge-transfer activity at nanoscale in the presence of UV-irradiation. However, more research works are needed to determine the optimize period and temperature of the UV-irradiation.

5) UV-resistant property of the APUS nanocomposite coating was significantly increased up to 98.77% with the incorporation of 2 wt% of APTMS-ZnO mixed with 2wt% corundum. While, 97.60% of UV-resistant was achieved in APUC with 6wt% of M–SiO_2 compared to APUC coating with individual nanoparticles. However, the samples with 6wt% M–SiO_2 nanoparticle showed derease in their visible light transparency and transmittance ability after 500 h of UV-irradiations.

6) The weathering stability of the nanoparticles embedded APUCs was significantly enhanced compared to neat PU film. Infact, it was observed that the tested samples with APTMS-ZnO and corundum nanoparticles have exhibited good wethering stability which means less weight loss and brittleness properties after 500 h of UV-irradiation compared to samples

with APMS-ZnO and SiO_2 nanoparticles. This might be due to the thermal stability of the corundum nanoparticle and the influence of the siloxane in the APUCs nanocomposite coating.

Acknowledgment

This research was funded by Ministry of Education Malaysia: FRGS grant no FP053-2015A and PR005-2017A; University Malaya research grants: PPP grant no PG159-2016A, RU grant no GPF033A-2018 and RU018H-2016 and ST012-2017.

Reference

[1] D. Tarasick, V. Fioletov, D. Wardle, J. Kerr, L. McArthur, C. McLinden, **Climatology and trends of surface UV radiation: Survey article,** Atmosphere-Ocean 41(2) (2003) 121-138.

[2] Y. Zhai, Y. Ma, S.N. David, D. Zhao, R. Lou, G. Tan, R. Yang, X. Yin, **Scalable-manufactured randomized glass-polymer hybrid metamaterial for daytime radiative cooling,** Science 355(6329) (2017) 1062-1066.

[3] H.J. Hrostowski, R. Kaiser, **Infrared absorption of oxygen in silicon,** Physical Review 107(4) (1957) 966.

[4] J.-H. Kim, K.-H. Lee, M.-J. Lee, J. Hwang, T.-Y. Lim, **Fabrication of ATO thin film for IR-cut off by sol-gel method,** Journal of the Korean Crystal Growth and Crystal Technology 23(5) (2013) 230-234.

[5] C. ZHANG, Q. ZHANG, T. JIANG, **Infrared blocking and heat insulation performance of polycarbonate enhanced by nano antimony doped tin oxide,** Acta Materiae Compositae Sinica 32(2) (2015) 365-369.

[6] E. Rephaeli, S. Fan, **Absorber and emitter for solar thermo-photovoltaic systems to achieve efficiency exceeding the Shockley-Queisser limit,** Optics express 17(17) (2009) 15145-15159.

[7] Y.X. Yeng, M. Ghebrebrhan, P. Bermel, W.R. Chan, J.D. Joannopoulos, M. Soljačić, I. Celanovic, **Enabling high-temperature nanophotonics for energy applications,** Proceedings of the National Academy of Sciences 109(7) (2012) 2280-2285.

[8] W.R. Chan, P. Bermel, R.C. Pilawa-Podgurski, C.H. Marton, K.F. Jensen, J.J. Senkevich, J.D. Joannopoulos, M. Soljačić, I. Celanovic, **Toward high-energy-density, high-efficiency, and moderate-temperature chip-scale thermophotovoltaics,** Proceedings of the National Academy of Sciences 110(14) (2013) 5309-5314.

[9] E. Rephaeli, A. Raman, S. Fan, **Ultrabroadband photonic structures to achieve high-performance daytime radiative cooling,** Nano letters 13(4) (2013) 1457-1461.

[10] A.P. Raman, M.A. Anoma, L. Zhu, E. Rephaeli, S. Fan, **Passive radiative cooling below ambient air temperature under direct sunlight,** Nature 515(7528) (2014) 540-544.

[11] T. Eriksson, A. Hjortsberg, C. Granqvist, **Solar absorptance and thermal emittance of Al_2O_3 films on Al: A theoretical assessment,** Solar Energy Materials 6(2) (1982) 191-199.

[12] E.N. Gribov, O. Zavorotynska, G. Agostini, J.G. Vitillo, G. Ricchiardi, G. Spoto, A. Zecchina, **FTIR spectroscopy and thermodynamics of CO and H_2 adsorbed on γ-, δ-and α-Al_2O_3,** Physical Chemistry Chemical Physics 12(24) (2010) 6474-6482.

[13] P.K. Sharma, M. Jilavi, D. Burgard, R. Nass, H. Schmidt, **Hydrothermal Synthesis of Nanosize alpha- Al_2O_3 from Seeded Aluminum Hydroxide,** Journal of the American Ceramic Society 81(10) (1998) 2732-2734.

[14] Y. Saito, T. Takei, S. Hayashi, A. Yasumori, K. Okada, **Effects of Amorphous and Crystalline SiO_2 Additives on γ- Al_2O_3- to- alpha- Al_2O_3 Phase Transitions,** Journal of the American Ceramic Society 81(8) (1998) 2197-2200.

[15] Z. Li, X. Feng, H. Yao, X. Guo, **Ultrafine alumina powders derived from ammonium aluminum carbonate hydroxide,** Journal of materials science 39(6) (2004) 2267-2269.

[16] R. Drumm, C. Goebbert, K. Gossmann, R. Nonninger, H. Schmidt, **Nanoscale corundum powders, sintered compacts produced from these powders and method for producing the same,** Google Patents, 2001.

[17] P.K. Kiyohara, H.S. Santos, A.C.V. Coelho, P.D.S. Santos, **Structure, surface area and morphology of aluminas from thermal decomposition of $Al(OH)(CH_3COO)_2$ crystals,** Anais da Academia Brasileira de Ciências 72(4) (2000) 471-495.

[18] B.E. Yoldas, **Hydrolysis of aluminium alkoxides and bayerite conversion**, Journal of Chemical Technology and Biotechnology 23(11) (1973) 803-809.

[19] T. Shirai, H. Watanabe, M. Fuji, M. Takahashi, **Structural properties and surface characteristics on aluminum oxide powders,** Ceramic Foundation Engineering Research Center Annual Report 9(23) (2009) 23-31.

[20] Y.-Q. Li, S.-Y. Fu, Y.-W. Mai, **Preparation and characterization of transparent ZnO/epoxy nanocomposites with high-UV shielding efficiency,** Polymer 47(6) (2006) 2127-2132.

[21] P. Katangur, P.K. Patra, S.B. Warner, **Nanostructured ultraviolet resistant polymer coatings,** Polymer degradation and stability 91(10) (2006) 2437-2442.

[22] Z. Han, X. Wang, C. Heng, Q. Han, S. Cai, J. Li, C. Qi, W. Liang, R. Yang, C. Wang, **Synergistically enhanced photocatalytic and chemotherapeutic effects of aptamer-functionalized ZnO nanoparticles towards cancer cells,** Physical Chemistry Chemical Physics 17(33) (2015) 21576-21582.

[23] J. Lee, S. Choi, S.J. Bae, S.M. Yoon, J.S. Choi, M. Yoon, **Visible light-sensitive APTES-bound ZnO nanowire toward a potent nanoinjector sensing biomolecules in a living cell,** Nanoscale 5(21) (2013) 10275-10282.

[24] J. Gangwar, B.K. Gupta, P. Kumar, S.K. Tripathi, A.K. Srivastava, **Time-resolved and photoluminescence spectroscopy of θ-Al_2O_3 nanowires for promising fast optical sensor applications,** Dalton transactions 43(45) (2014) 17034-17043.

[25] A. Jaramillo, R. Baez-Cruz, L. Montoya, C. Medinam, E. Pérez-Tijerina, F. Salazar, D. Rojas, M. Melendrez, **Estimation of the surface interaction mechanism of ZnO nanoparticles modified with organosilane groups by Raman Spectroscopy,** Ceramics International 43(15) (2017) 11838-11847.

[26] L. Zhang, M. Zhong, H. Ge, **Surface modification of zinc oxide nanorods for potential applications in organic materials,** Applied Surface Science 258(4) (2011) 1551-1554.

[27] R. Hong, J. Li, L. Chen, D. Liu, H. Li, Y. Zheng, J. Ding, **Synthesis, surface modification and photocatalytic property of ZnO nanoparticles,** Powder Technology 189(3) (2009) 426-432.

[28] R. Ishii, H. Mori, K. Matsumura, N. Hongo, H. Kiyosue, S. Matsumoto, T. Yoshimi, S. Ujiie, **Molecular interactions between anticancer drugs and iodinated contrast media: An in vitro spectroscopic study,** Journal of Biomedical Science and Engineering 5(01) (2012) 24.

[29] Y. Zhu, T.L. Tan, **Penalized discriminant analysis for the detection of wild-grown and cultivated Ganoderma lucidum using Fourier transform infrared spectroscopy,** Spectrochimica Acta Part A: Molecular and Biomolecular Spectroscopy 159 (2016) 68-77.

[30] P. Maynard, K. Gates, C. Roux, C. Lennard, **Adhesive tape analysis: establishing the evidential value of specific techniques,** Journal of Forensic Science 46(2) (2001) 280-287.

[31] W. Wang, C. Chen, C. Tollan, F. Yang, Y. Qin, M. Knez, **Efficient and controllable vapor to solid doping of the polythiophene P3HT by low temperature vapor phase infiltration,** Journal of Materials Chemistry C 5(10) (2017) 2686-2694.

[32] Y.C. Ching, I.I. Iskander, **Effect of Polyurethane/nanosilica composites coating on thermo-mechanical properties of polyethylene film,** Materials Technology 27(1) (2012) 113-115.

[33] T. Sandutsa, N. Kvasman, N. Pisareva, A. Gaodu, E. Degtyareva, **Optimizing the properties of corundum-based thermal insulation products using the method of experimental planning,** Refractories and Industrial Ceramics 28(5) (1987) 310-313.

[34] H. Tippins, **Charge-transfer spectra of transition-metal ions in corundum,** Physical Review B 1(1) (1970) 126.

[35] E.-C. Lee, K. Chang, **Electrically inactive nitrogen complex in Si oxynitride,** Physical Review B 66(23) (2002) 233205.

[36] N. Sheppard, D.C. Yates, **Changes in the infra-red spectra of molecules due to physical adsorption,** Proceedings of the Royal Society of London A: Mathematical, Physical and Engineering Sciences, The Royal Society, 1956, pp. 69-89.

[37] Y.C. Ching, N. Kalyani, M. Khalid, W. Yoong, **Optical and structural characterization of solution processed zinc oxide nanorods via hydrothermal method,** Ceramic International 40 (2014) 9997- 10004.

[38] Y.C. Ching, S Nurehan, **Effect of nanosilica filled polyurethane composite coating on polypropylene substrate.** Journal of Nanomaterials Volume 2013, Article ID 567908 http://dx.doi.org/10.1155/2013/567908.

[39] Y.C. Ching, K.Y, Goh, C.A. Luqman, Kalyani, N. **Effect of nanosilica and titania on thermal stability of polypropylene/oil palm empty fruit fibre composite,** Journal of Biobased Materials and Bioenergy 7 (2013) 169-174

[40] Y. Jiang, Y. Song, M. Miao, S. Cao, X. Feng, J. Fang, L. Shi, **Transparent nanocellulose hybrid films functionalized with ZnO nanostructures for UV-blocking,** Journal of Materials Chemistry C 3(26) (2015) 6717-6724.

[41] J. Guan, Y. Song, Y. Lin, X. Yin, M. Zuo, Y. Zhao, X. Tao, Q. Zheng, **Progress in study of non-isocyanate polyurethane,** Industrial & Engineering Chemistry Research 50(11) (2011) 6517-6527.

42] Z. Wang, X. Zhan, Y. Wang, S. Muhammad, Y. Huang, J. He, **A flexible UV nanosensor based on reduced graphene oxide decorated ZnO nanostructures,** Nanoscale 4(8) (2012) 2678-2684.

[43] Y. Ren, M. Chen, Y. Zhang, L. Wu, **Fabrication of rattle-type TiO_2/SiO_2 core/shell particles with both high photoactivity and UV-shielding property,** Langmuir 26(13) (2010) 11391-11396.

[44] Y.C. Ching, I.Y. Iskandar, **Influence of Nano-SiO2/Polyamide composites coating on thermic effect and optical properties of polyethylene film**, International Journal of Modern Physics B 23(6-7) (2009) 1395-1400

[45] R. Ashiqur, Y.C. Ching, Y.C. Kuan, N. Awanis, A.C. Ashok, H.C. Cheng, L. N. Shang, **Surface modification of natural fiber using Bi2O3/TiO2 composite for photocatalytic self- cleaning**. BioResource 10(4) (2015) 7405-7418.

[46] Y.C. Ching, I.Y. Iskandar, W**eathering effect on virgin PE & PE coated with Polyamide/nanosilica composite coating**, Journal of Computational and Theoretical Nanoscience 9(2012) 1-4.